Proteomic Analysis Reveals a Role for RSK in p120-catenin Phosphorylation and Melanoma Cell-Cell Adhesion

Authors

Antoine Méant, Beichen Gao, Geneviève Lavoie, Sami Nourreddine, Flora Jung, Léo Aubert, Joseph Tcherkezian, Anne-Claude Gingras, and Philippe P. Roux

Correspondence

philippe.roux@umontreal.ca

In Brief

The p90 ribosomal S6 kinase (RSK) family contains four related members with roles in cancer. The proximity-dependent biotinylation (BioID) approach was used to reveal their biological functions. Several proximity partners were identified, including p120ctn, an essential component of adherens junctions. The results reported reveal a role for RSK in p120ctn phosphorylation and in the regulation of adherens junctions.

Graphical Abstract
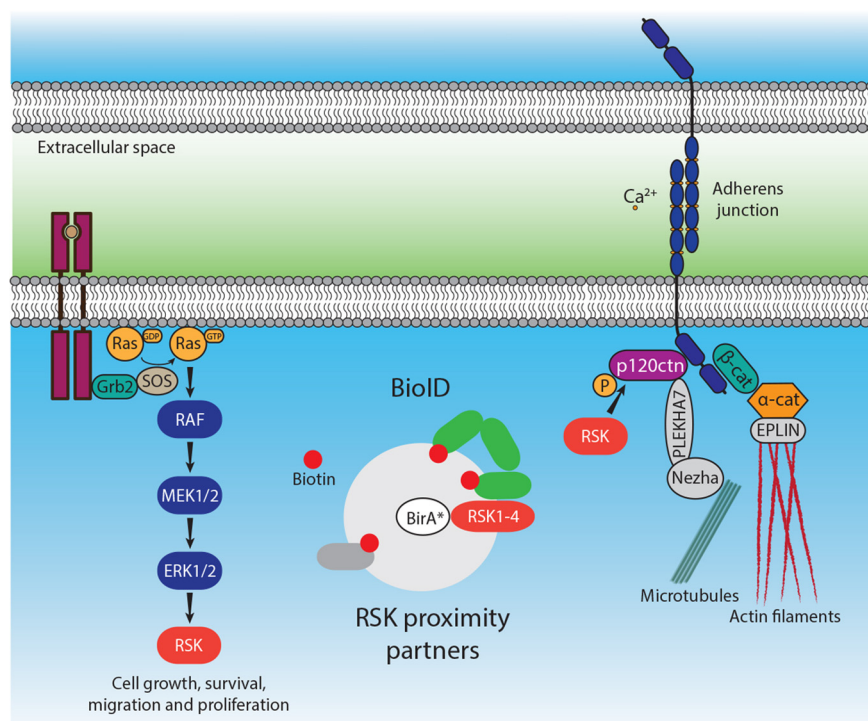
Highlights

- BioID reveals the proximity partners of RSK family members.

- All RSK isoforms associate with and phosphorylate p120ctn on Ser320.

- RSK negatively regulates adherens junctions and reduces cell-cell adhesion.

- p120ctn phosphorylation plays a role in the reorganization of proximity partners.

Proteomic Analysis Reveals a Role for RSK in p120-catenin Phosphorylation and Melanoma Cell-Cell Adhesion*⑤

Antoine Méant‡, Beichen Gao‡, Geneviève Lavoie‡, Sami Nourreddine‡, Flora Jung‡, Léo Aubert‡, Joseph Tcherkezian‡, ⑩ Anne-Claude Gingras§¶, and ⑩ Philippe P. Roux‡‖**

The RAS/mitogen-activated protein kinase (MAPK) signaling pathway regulates various biological functions, including cell survival, proliferation and migration. This pathway is frequently deregulated in cancer, including melanoma, which is the most aggressive form of skin cancer. RSK (p90 ribosomal S6 kinase) is a MAPK-activated protein kinase required for melanoma growth and proliferation, but relatively little is known about its function and the nature of its cellular partners. In this study, we used a proximity-based labeling approach to identify RSK proximity partners in cells. We identified many potential RSK-interacting proteins, including p120ctn (p120-catenin), which is an essential component of adherens junction (AJ). We found that RSK phosphorylates p120ctn on Ser320, which appears to be constitutively phosphorylated in melanoma cells. We also found that RSK inhibition increases melanoma cell-cell adhesion, suggesting that constitutive RAS/MAPK signaling negatively regulates AJ integrity. Together, our results indicate that RSK plays an important role in the regulation of melanoma cell-cell adhesion. *Molecular & Cellular Proteomics 19: 50–64, 2020. DOI: 10.1074/mcp.RA119.001811.*

The RAS/mitogen-activated protein kinase (MAPK)[1] signaling cascade plays a key role in transducing extracellular signals to intracellular targets involved in a wide range of cellular functions, including cell growth, proliferation and survival (1, 2). Inappropriate regulation of this pathway leads to a variety of disorders and diseases, including many types of cancers (3, 4). Upon activation by upstream RAS isoforms or in response to mutational activation, RAF phosphorylates and activates MEK1/2, which then phosphorylate and activate ERK1/2 (5, 6). RAF isoforms are frequently mutated in cancers and one major example is melanoma, which harbors activating B-Raf mutations (V600E) in most cases (7). Once activated, ERK1/2 phosphorylate many substrates, including

members of the p90 ribosomal S6 kinase (RSK) family of proteins (8, 9).

The RSK family includes four Ser/Thr kinases (RSK1–4) that belong to the AGC family of basophilic protein kinases (10). Although RSK1 and RSK2 are ubiquitously expressed, RSK3 and RSK4 were shown to be expressed in a tissue-specific manner (9). RSK1–4 display high sequence identity within their kinase domains, but differences at their amino- and C-terminal regions suggest that they regulate specific cellular functions. Although several phosphorylation substrates have been identified for RSK1 and RSK2, the exact functions of RSK3 and RSK4 remain elusive. RSK1 and RSK2 have been shown to regulate cell growth, cell survival, proliferation and motility (11–14). Consistent with this, RSK1 and RSK2 were shown to be overexpressed and/or hyperactivated in many types of cancers, including breast cancer (15), prostate cancer (16), head and neck squamous cell carcinoma (HNSCC) (17), and melanoma (18). Accordingly, inhibition of RSK activity reduces the proliferation of several cancer cell lines (19, 20). Conversely, reduced expression of RSK3 and/or RSK4 has been observed in different cancer types (21, 22), suggesting that these proteins could act as potential tumor suppressors (23).

Loss of cell-cell adhesion is frequently observed in many disorders upon dysfunction of cadherins, the major component of adherens junction (AJ) (24). Cadherins constitute a family of transmembrane cell-cell adhesion proteins involved in morphogenesis, development and cancer (25). Classical cadherins are the gatekeepers of AJ maintenance by linking their extracellular interactions to internal cellular elements through α-catenin, β-catenin and p120-catenin (p120ctn) (26). Although α- and β-catenin mainly modulate functional interactions with the actin cytoskeleton, p120ctn maintains cell-cell adhesion integrity by controlling the stability of cadherins at the plasma membrane (27–29). p120ctn is a member of the

Armadillo-repeat (ARM) protein family and was originally identified as a Src tyrosine kinase substrate (30). To date, several other p120ctn residues have been shown to be phosphorylated, suggesting the regulation of p120ctn phosphorylation by other kinases (31). Interestingly, the phosphorylation status of p120ctn seems to regulate AJ assembly, specifically by controlling cadherin dynamics at the plasma membrane (32, 33). Finally, although the down-regulation or change in localization of p120ctn has been demonstrated in many cancers, several cases suggest that p120ctn phosphorylation is required for its pro-tumorigenic potential (34, 35). Thus, the role and regulation of p120ctn phosphorylation remain to be clearly defined.

In this study, we used a proximity-based labeling approach (BioID) to identify proximity partners of the RSK isoforms. This proteomic approach resulted in the identification of many potential cellular partners for the RSK kinases. Among them, we identified and characterized p120ctn as RSK phosphorylation substrate. After demonstrating the direct impact of p120ctn on cell-cell junctions in melanoma, we found that RSK kinase activity negatively regulates AJ integrity. We found that RSK phosphorylates p120ctn at Ser320, which appears to reorganize its global proximity partners. Together, these results help understand the specific roles of the RSK kinases, particularly with respect to their described functions in cancer.

EXPERIMENTAL PROCEDURES

Antibodies—Antibodies targeted against the Arg-X-X-pSer/Thr motif (#9614), phospho-p120ctn (S320) (#8016), Akt (#9262) and phospho-Akt (S473) (#4051), ERK1/2 (#4695) and phospho-ERK1/2 (T202/Y204) (#9101), S6K (#9202) and phospho-S6K (T389) (#9205), rps6 (#2217) and phospho-rps6 (S235/236) (#2211) were purchased from Cell Signaling Technologies (Beverly, MA). RSK1 (sc-81162), RSK2 (sc-9986), 4E-T (393788) and p120ctn (sc-373751) antibodies were purchased from Santa Cruz Biotechnologies (Santa Cruz, CA). The N-cadherin antibody (#561553) was purchased from BD Biosciences (San Jose, CA). Anti-myc (#M4439), anti-tubulin (#T6199), anti-Flag (#MAB3118) and anti-HA (#H9658) monoclonal antibodies were purchased from Sigma-Aldrich (Oakville, Ontario, Canada).

DNA Constructs—The original plasmid encoding full-length, untagged p120ctn was kindly provided by Albert Reynolds (Vanderbilt University, Nashville) in a pENTR-gateway plasmid backbone (pENTR-p120ctn-1AB). This DNA construct was used as template for generating 6×Myc-tagged p120ctn in the pcDNA3.1 backbone. Both p120ctn mutants (S320A and S320D) were generated using the QuikChange methodology (Stratagene, La Jolla, CA). The original plasmid pcDNA5-FRT/TO-FLAG-BirA$_{R118G}$ encoding Flag-tagged BirA$_{R118G}$ was provided by Anne-Claude Gingras (University of Toronto, Toronto, Canada). The plasmid pLenti-CMV-GFP-puro was obtained from Addgene (#17448, Cambridge, MA).

Cell Culture and Transfection—HEK293, A375 and Colo829 cells were obtained from the American Type Culture Collection (ATCC). HEK293 and A375 cells were maintained at 37 °C in Dulbecco's modified Eagle medium (DMEM) with 4.5 g/L glucose supplemented with 5% (v/v) FBS, 100 IU/ml penicillin, and 100 μg/ml streptomycin. Colo829 cells were grown in RPMI 1640 medium with similar supplements. Cells were regularly PCR tested to exclude mycoplasma contamination and used within 2 months after thawing. HEK293 cells were transfected by calcium phosphate 24h after being plated, done previously (36). Cells were grown for 24h after transfection and serum-starved overnight using serum-free DMEM where indicated. Starved cells were pretreated with PD184352 (10 μM; Cerdalane, ON, Canada), LJH685 (10 μM; Selleckchem, TX), BI-D1870 (10 μM; Selleckchem, TX), SL0101 (50 μM; Toronto Research Chemicals, ON, Canada), PI-103 (1 μM; Calbiochem, CA), rapamycin (25 nM; Calbiochem, CA) or Ku-0063794 (10 μM; Selleckchem, TX) where indicated and stimulated with phorbol 12-myristate 13-acetate (PMA; 100 ng/ml; Fisher Scientific, ON, Canada), EGF (25 ng/ml: Invitrogen, CA), FBS (10%; Invitrogen, CA) or insulin (100 nM; Peprotech, NJ) before being harvested.

RNA Interference (RNAi) and Viral Infections—Short hairpin RNA (shRNA)-mediated knockdown was achieved using lentiviruses produced with vectors from the Mission TRC shRNA library (p120ctn, TRCN0000122984, TRCN0000122987; RSK1, TRCN0000001388; RSK2, TRCN0000040143). Cells were infected in the presence of 4 μg/ml polybrene, and 3 days after viral infection, A375 and Colo829 cells were treated and selected with 2 μg/ml puromycin. Lentiviruses were produced in the HEK293T cell line using the pLenti-CMV-GFP-puro vector to overexpress ectopic GFP, p120ctn WT, S320A, or S320D mutants. Two days after infection, cells were selected with 2 μg/ml puromycin.

Immunoprecipitations, Kinase Assay and Immunoblotting—Cells were washed three times with ice-cold phosphate-buffered saline (PBS) and lysed in BLB (10 mM K$_3$PO$_4$, 1 mM EDTA, 5 mM EGTA, 10 mM MgCl$_2$, 50 mM β-glycerophosphate, 0.5% Nonidet P-40, 0.1% Brij 35, 0.1% deoxycholic acid, 1 mM sodium orthovanadate [Na$_3$VO$_4$], 1 mM phenylmethylsulfonyl fluoride, and a complete protease inhibitor mixture tablet [Roche]). For cell fractionation, the total homogenate was centrifuged at 14,000 × g to generate soluble and insoluble fractions. For immunoprecipitations, soluble cell lysates were incubated with the indicated antibodies for 2 h, followed by 1 h of incubation with protein A-Sepharose CL-4B beads (GE Healthcare). Immunoprecipitates were washed three times in lysis buffer, and beads were eluted and boiled in 2× reducing sample buffer (5× buffer is 60 mM Tris-HCl [pH 6.8], 25% glycerol, 2% SDS, 14.4 mM 2-mercaptoethanol, and 0.1% bromphenol blue). For kinase assay, immunoprecipitates were washed three times in lysis buffer followed by one wash in kinase buffer (25 mM Tris-HCl (pH 7.4), 10 mM MgCl$_2$, and 5 mM β-glycerophosphate). Then, recombinant activated RSK2 purchased from SignalChem (Richmond, BC) was used with immunoprecipitated p120ctn as substrate (WT and S320A) under linear assay conditions. Assay was performed for 10 min at 30 °C in kinase buffer and then stopped by adding 2× reducing sample buffer. Eluates and total cell lysates were subjected to 10% SDS-PAGE, and resolved proteins were transferred onto polyvinylidene difluoride membranes for immunoblotting.

Immunofluorescence Microscopy—For immunofluorescence analysis, HEK293 or A375 cells were seeded in 12-well plates containing coverslips. Twenty-four to 72 h later, cells were washed twice in PBS and fixed in 3.7% formaldehyde for 10 min at room temperature. Cells were washed twice in PBS, permeabilized for 5 min in PBS containing 0.3% Triton X-100 and blocked with PBS containing 1% bovine serum albumin (BSA) for 30 min. Cells were incubated for 1 or 2 h with primary antibodies, washed twice with PBS, and incubated for 1 h

---

with secondary Alexa Fluor 488-conjugated goat anti-rabbit and Alexa Fluor 555-conjugated goat anti-mouse antibodies (Invitrogen), Texas Red-phalloidin, and DAPI (4,6-diamidino-2-phenylindole) diluted in PBS. Images were acquired on a Zeiss Axio Imager Z1 wide-field fluorescence microscope using a 40X oil-immersion objective (Fig. 1), a Deltavision microscope (Applied Precision, Issaquah, WA) using a 60X oil-immersion objective (Fig. 5), or a Zeiss LSM 700 confocal microscope (PlanApo 63x aperture) (Fig. 6 and 7).

Tissue Microarray (TMA)—Immunohistochemical staining against p120ctn phospho-S320 was carried out on paraffin-embedded formalin-fixed samples using the automated Bond RX staining platform from Leica Biosystems. Sections were deparaffinized inside immunostainer. Antigen recovery was conducted using heat retrieval (Heat-Induced Epitope Retrieval) with ER1 (Leica Biosystems proprietary Epitope Retrieval using a low pH buffer) for 20 min. Sections were then incubated with 150 μl of anti-p120ctn phospho-S320 antibody for 30 min at room temperature. Detection of specific signal was acquired by using Bond Intense R detection kit (#DS9263; Leica Biosystems) according to the provider's recommendations. Slides were counterstained automatically with hematoxylin included in the Polymer DAB Kit. Stained slides were scanned using the Hamamatsu's Nano Zoomer Digital Pathology system 2HT. Virtual slides were then imported in Visiopharm Integrator System (3.4.1.0). Scanned tissue microarray was processed by using the array imager module. Then each core was classified using Visiomorph's K-Means clustering method. CMN biomarker scoring algorithm was applied. VS = $(MI \times Area)_{LOW} + (MI \times Area)_{MED} + (MI \times Area)_{STRONG}$/Total Area of ROI. *versus* (Global visiomorph score) is range between 0 and + 255, MI (average intensity).

Mechanical Strength (Dispase) Assay—A375 cells were plated in 60 mm cell culture plates to reach confluency within 72 h. To isolate the monolayers from the plates, cells were washed twice with PBS and then incubated for 90 min at 37 °C with media containing Dispase (2.4U/ml, Roche). After detachment, PBS was added slowly to fully release the monolayer and the suspended cells were then centrifuged at 1000 rpm for 5 min. Each monolayer was then subject to disruption by pipetting up and down 20 times in 1 ml PBS. Immediately after disruption, single cells were counted using a hemocytometer. Percentage fragmentation was calculated by determining the ratio of single cell compared with the total number of cells present in a 60 mm cell culture plate for each condition. In experiments requiring inhibitors, cells were treated with medium containing PD184352 (10 μM), LJH685 (10 μM) or DMSO (solvent control) 24 h prior to performing the assay.

Generation of Stable Inducible Cell Pools and BioID Labeling—Stable cell lines were generated in parental HEK293 Flp-In T-Rex cells expressing bait proteins of interest, as described (37). Stable cell lines were selectively grown in the presence of 200 μg/ml hygromycin up to 80% confluence before expression was induced using 1 μg/ml tetracycline for 24 h. For the BioID experiments, 50 μM biotin was added at the time of induction. Two 150-mm plates were induced with tetracycline and treated with biotin for 24 h before harvesting. Cells were pelleted at low speed, washed with ice-cold PBS and frozen at −80 °C until purification. Cell pellets were thawed in 1.5 ml ice cold RIPA buffer containing 20 mM Tris-HCl (pH 8), 137 mM NaCl, 1% NP-40, 0.1% SDS and 0.5% sodium deoxcycholate. 1 mM phenylmethylsulfonyl fluoride, 1 mM dithiothreitol and a complete protease inhibitor mixture tablet (Roche, Basel, Switzerland) were added immediately before use, supplemented with 250U of benzonase. The lysates were sonicated using three 10 s bursts with 10 s rest in between on ice at 20% amplitude. Lysates were centrifuged for 20 min and cleared supernatants were transferred to 2-ml microcentrifuge tubes, and a 60 μl bed volume of prewashed streptavidin-agarose beads (GE Healthcare) was added to each sample. Affinity

purification was performed at 4 °C on a nutator for 3 h, and the beads were washed twice in RIPA buffer, and three times in 50 mM ammonium bicarbonate (ABC; pH 8.0). After affinity purification and removal of all washing buffer, beads were resuspended in 100 μl of 50 mM ABC (pH 8) with 1 μg of trypsin (Sigma) added and incubated at 37 °C overnight with agitation. The next day, an additional 1 μg of trypsin was added to each sample, and the samples were incubated for 4 h at 37 °C. Beads were pelleted, and the supernatant was transferred to a fresh 1.5-ml tube. The beads were then rinsed two times with 100 μl of MS-grade H_2O, and these rinses were combined with the original supernatant. The pooled fractions were centrifuged, and the supernatant was transferred to a new 1.5-ml tube and dried in a vacuum centrifuge. Tryptic peptides were resuspended in 10 μl of 5% formic acid.

Mass Spectrometry Acquisition and Data Analysis—Samples were reconstituted in formic acid 0.2% and loaded and separated on a homemade reversed-phase column (150 μm i.d. × 150 mm) with a 56-min gradient from 0–40% acetonitrile (0.2% FA) and a 600 nl/min flow rate on an Easy-nLC II (Thermo Fisher Scientific), connected to an Orbitrap Fusion Tribrid mass spectrometer (Thermo Fisher Scientific). Each full MS spectrum acquired with a 60,000 resolution was followed by 20 MS/MS spectra, where the 12 most abundant multiply charged ions were selected for MS/MS sequencing. Samples analyzed were converted to mzXML using ProteoWizard 3.0.4468 (38) and analyzed using the iProphet pipeline (39) implemented within ProHits (40). The database consisted of the human and adenovirus sequences in the RefSeq protein database (version 57) supplemented with "common contaminants" from the Max Planck Institute (http://maxquant.org/downloads.htm) and the Global Proteome Machine (GPM; http://www.thegpm.org/crap/index.html). The sequence database consisted of forward and reversed sequences; 72,226 entries searched. The search engines were Mascot (2.3.02; Matrix Science) and Comet (2012.01 rev.3 (41)), with trypsin specificity and two missed cleavage sites allowed. Methionine oxidation and asparagine/glutamine deamidation were set as variable modifications. The fragment mass tolerance was 0.01 Da and the mass window for the precursor was ± 10 ppm. The resulting Comet and Mascot results were individually processed by PeptideProphet (42) and combined into a final iProphet output using the Trans-Proteomic Pipeline (TPP; Linux version, v0.0 Development trunk rev 0, Build 201303061711). TPP options were as follows. General options were -p0.05 -x20 -PPM -d"DECOY", iProphet options were pPRIME and PeptideProphet options were pP. All proteins with a minimal iProphet protein probability of 0.05 were parsed to the relational module of ProHits. Note that for analysis with SAINTexpress, only proteins with at least two peptides identify and with iProphet protein probability ≥ 0.95 are considered. This corresponds to an estimated protein level FDR of ~0.5%.

Proximity interaction scoring was done using SAINTexpress version 3.6.1 for p120ctn, and version 3.3 for RSK (43) using default parameters. For the RSK and p120ctn datasets, the 9 controls were compressed to 3 virtual controls to increase stringency in scoring, as first performed in (44); the 3 biological replicates for each bait were compressed to the best two to increase sensitivity in scoring. Interaction data visualization was with Cytoscape (version, reference) or with using the default parameters in ProHits-viz (45).

All MS data was deposited in ProteomeXchange through partner MassIVE as a complete submission (supplemental Tables S1, S2, S3*A* and S3*B*) and assigned MSV000083414 and PXD012619. It can be downloaded from ftp://MSV000083414@massive.ucsd.edu.

Digestion, Phosphorylation Site Identification and Quantification—Following SDS-PAGE separation with Coomassie staining, bands corresponding to p120ctn were excised and digested in gel with trypsin as previously described (46). The tryptic peptides were analyzed as described above. Database searches were performed using

Mascot (2.3.02; Matrix Science). The fragment mass tolerance was 0.01 Da and the mass window for the precursor was $\pm$ 10 ppm. Assignment of phosphorylation sites were validated through manual inspection of relevant MS/MS spectra. Individual sites were quantified based on the summed reporter ion intensities for all matching peptides. Non-phosphorylated peptides matching p120ctn were combined to estimate unmodified protein abundance.

Experimental Design and Statistical Rationale—For each BioID experiment, biological triplicates were employed (each replicate generated through independent harvests). Statistical scoring was performed against 9 negative controls compressed to 3 virtual controls using Significance Analysis of INTeractome (SAINT; SAINTexpress 3.6.1 was employed for p120ctn, and SAINTexpress 3.3 for RSK) as described above. Control samples are described above. The average SAINTexpress score was used to determine the Bayesian FDR, which therefore requires a high confidence interaction to be detected across at least two of the biological replicates. For the remainder of the manuscript, statistical analyses were performed using a two-sample unequal-variance Student t test. Data are presented as the mean $\pm$ S.E., and p values $<$ 0.05 were statistically significant. Data are representative of results from at least three independent experiments.

RESULTS

Global Analysis of Cellular RSK Proximity Partners—To characterize the proximity partners of the RSK isoforms, we conducted a proximity-dependent biotin identification (BioID) screen in HEK293 cells, as done elsewhere (47). For this, RSK1–4 were fused in-frame with a promiscuous form (R118G) of the biotin ligase BirA (BirA*) (Fig. 1A). Each bait was stably integrated in the tetracycline-inducible Flp-In T-Rex HEK293 cell system, and additional control cell lines (No BirA*, BirA*, BirA*-GFP) were generated to facilitate data analysis. The addition of tetracycline and exogenous biotin led to the expression of the bait and protein biotinylation, respectively (Fig. 1B). All baits appeared to be expressed to similar levels and to the appropriate cellular compartments (Fig. 1C). RSK1 and RSK3 were found to associate with insoluble material following cell lysis with non-ionic detergents (Fig. 1D), underscoring the need to use an *in vivo* proximity labeling approach to assess their potential interacting partners. For mass spectrometry (MS) analysis, cells were lysed and biotinylated proteins were isolated using streptavidin-agarose affinity capture. BioID coupled with MS was performed in biological triplicates on these baits grown under standard conditions (Fig. 1A). SAINTexpress (43) was used to define high-confidence proximity interactions for each of the bait proteins, and only high-confidence interactions (SAINT score $\geq$ 0.85 and FDR $\leq$ 0.05, as statistical cut-off) were considered further.

Using this approach, we identified 156 prey proteins as RSK proximity partners (Fig. 2A, supplemental Tables S3A, S4). Most proteins were identified with RSK1 and RSK3 as baits, likely because of their localization to more specific subcellular compartments (Fig. 1C–1D). To characterize the global signature of identified proximity partners, we used the Ingenuity Pathway Analysis platform (IPA). When analyzed together, we found that RSK proximity partners were enriched in specific cellular compartments, including cell junction ($p = 2.44 \times 10^{-9}$), anchoring junction ($p = 1.12 \times 10^{-8}$) and plasma membrane ($p = 5.92 \times 10^{-7}$) (Fig. 2B–2C). According to BioGRID (https://thebiogrid.org/) (48), we identified 7 known RSK interacting proteins, including ERK1 and ERK2. We also identified known RSK substrates, such as ARH-GEF12 (49) and EPHA2 (50), suggesting that the RSK proximity interactome may also contain uncharacterized RSK substrates. Consistent with this possibility, we compared these data with a list of potential RSK substrates identified in a recent phosphoproteomic study (18), and found that at least 10 proximity partners were previously tagged as potential RSK substrates (Fig. 2D), including p120-catenin (p120ctn or CTNND1).

Identification of p120ctn As A Substrate of the RSK Protein Kinases—RSK is a basophilic protein kinase that operates downstream of the RAS/MAPK pathway (9). To test its potential involvement in the regulation of p120ctn phosphorylation, we first used an antibody that recognizes the RXXpS/T (where X is any amino acid) consensus motif, which is typically phosphorylated by AGC family kinases such as RSK (51). HEK293 cells transfected with Myc-tagged human p120ctn were stimulated with phorbol 13-myristate 12-acetate (PMA), and immunoprecipitated p120ctn was analyzed for phosphorylation (Fig. 3A). Using this method, we found that acute PMA treatment strongly stimulated p120ctn phosphorylation on RXXpS/T consensus sites, which was prevented by treatments with either MEK1/2 (PD184352) or RSK (BI-D1870) inhibitors. We found that expression of RSK1–4 promotes p120ctn phosphorylation on RXXpS/T consensus sites (Fig. 3B), suggesting that all four RSK isoforms have the potential to promote p120ctn phosphorylation. To identify the exact phosphorylation site(s) regulated by RSK, we used an MS-based approach. As above, HEK293 cells were transfected with Myc-tagged p120ctn, serum-starved overnight, and pre-treated with vehicle, MEK1/2 or RSK inhibitors prior to being stimulated with PMA. Immunoprecipitated p120ctn was isolated via SDS-PAGE and digested in-gel with trypsin. Samples were then analyzed by liquid chromatography-assisted tandem MS, and the relative abundance of all identified phosphopeptides was measured across experimental conditions. Using this approach, we found that one phosphopeptide containing a RSK motif showed significant changes between resting (vehicle), activated (PMA) and inactivated (PD184352 or BI-D1870) conditions (Fig. 3C). This phosphopeptide was found to contain Ser320, and identification of this residue as being phosphorylated was obtained by MS/MS sequencing, as depicted by the annotated MS/MS spectra. Using a phosphospecific antibody targeted against Ser320, we confirmed that expression of all RSK isoforms promotes p120ctn phosphorylation at this site (Fig. 3D). Consistent with this, we found that all four RSK isoforms co-immunoprecipitate with p120ctn (Fig. 3E). In order to confirm that Ser320 phosphorylation is RSK-dependent, we generated a non-phosphorylatable
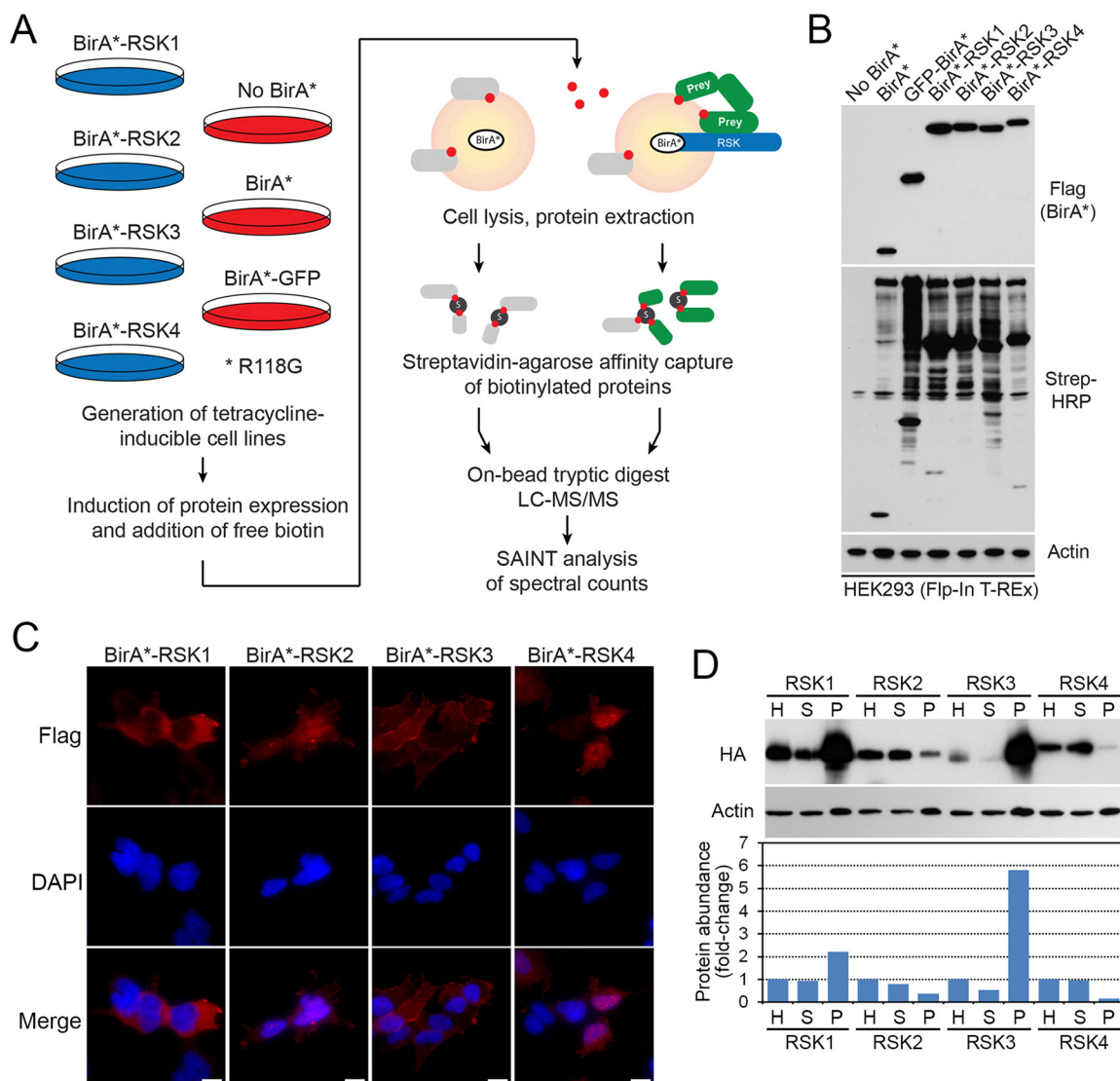
Fig. 1. **Proteomic strategy to identify RSK proximity partners.** *A*, Schematic representation of the different bait proteins analyzed using BioID. Each RSK isoforms was fused at its N-terminus with a Flag epitope followed by the mutant *E. coli* biotin conjugating protein BirA-R118G (BirA*) in a tetracycline inducible system. In the presence of tetracycline and biotin, the expressed baits were allowed to biotinylate proximity cellular components on lysine residues. Following cell lysis using stringent conditions, biotinylated proteins were affinity-purified using streptavidin beads. Streptavidin-bound proteins were washed and subjected to trypsin proteolysis, and the peptides were identified using LC-MS/MS. *B*, HEK293 Flp-In T-REx stable cell lines were treated with tetracycline in the presence of biotin for 24 h to induce bait expression and proximity biotinylation. Bait expression and associated biotinylation patterns were monitored using Flag antibodies and streptavidin-HRP, respectively. *C*, HEK293 Flp-In T-REx stable cell lines expressing bait proteins were imaged using immunofluorescence microscopy. Cells were stained with Flag antibodies and DAPI to visualize nuclei. Scale bars, 10 μm. *D*, HEK293 cells transfected with HA-tagged RSK1–4 were lysed using non-ionic detergents. Homogenate cell lysates were divided into three different fractions (H, Homogenate; S, Soluble; P, Pellet). Immunoblotting results were quantified for intensity using MultiGauge software.

p120ctn mutant (S320A). Importantly, we found that mutation of Ser320 completely abrogated p120ctn phosphorylation at basic consensus motifs in response to PMA (Fig. 3*F*) and EGF (Fig. 3*G*) stimulation. We also performed *in vitro* kinase assays with purified proteins. Recombinant active RSK2 was incubated in a kinase reaction buffer with immunoprecipitated p120ctn WT or the S320A mutant (Fig. 3*H*). We found that activated RSK2 increased the phosphorylation of immunoprecipitated p120ctn WT, but not the S320A mutant. Taken together, these results

indicate that Ser320 is the predominant RSK-dependent phosphorylation site in p120ctn. Interestingly, Ser320 is located within the regulatory domain of p120ctn (Fig. 3*I*), suggesting that its phosphorylation may modulate p120ctn function in cells. Ser320 appears to be evolutionarily conserved among vertebrate species (Fig. 3*J*), suggesting that this phosphorylation event may play important regulatory roles.

RSK is Required for p120ctn Phosphorylation in Cells—To assess the regulation of Ser320 in cells, we used a phospho-
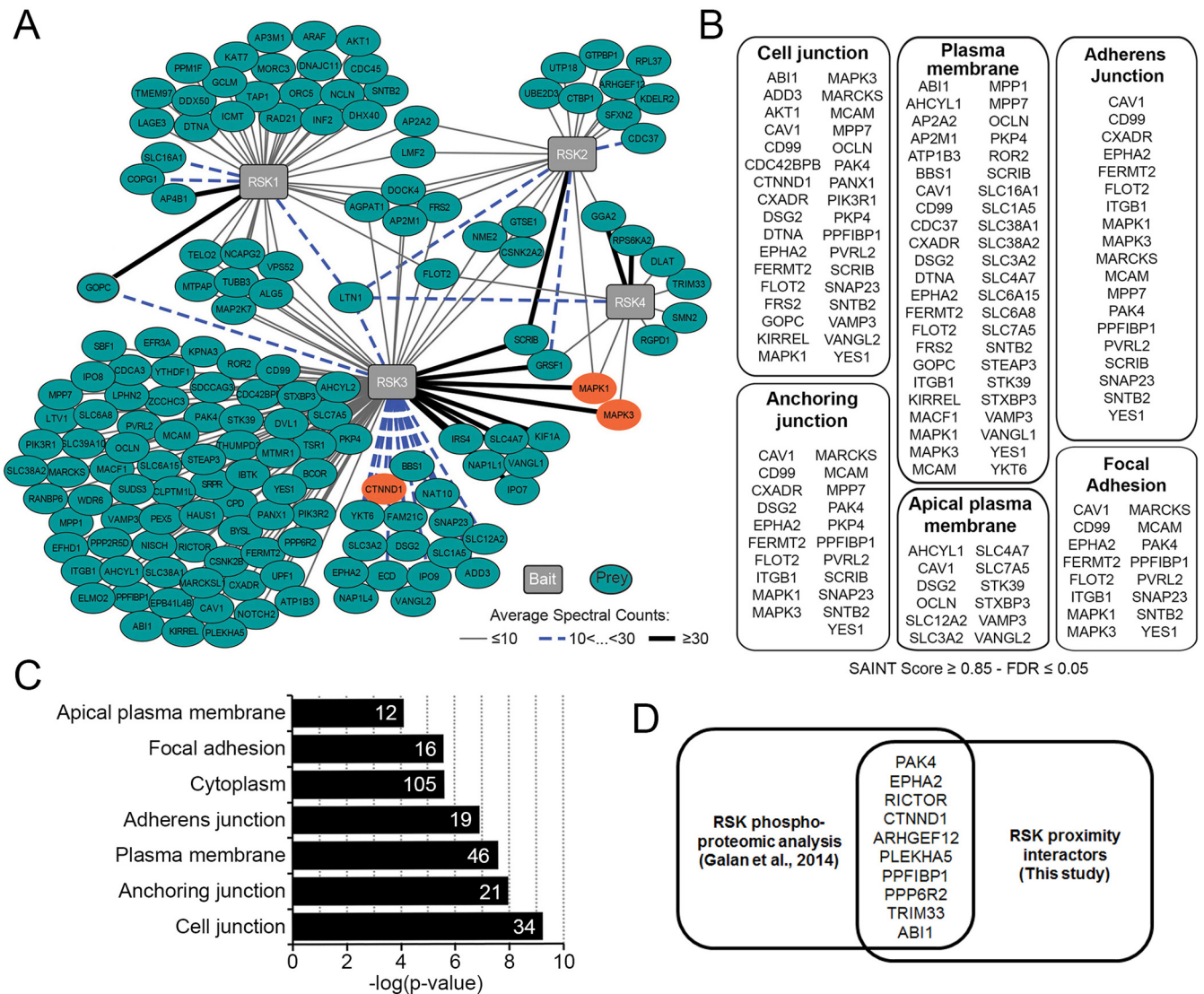
FIG. 2. **Characterization of the RSK proximity partners.** *A*, Detailed proximity interactions for all preys identified by BioID. Proximity partners are organized with respect to associated baits, and relative levels are shown using normalized spectral counts. Upstream protein kinases ERK1 (MAPK1) and ERK2 (MAPK3) are shown in orange, as well as the interactor analyzed in this study (CTNND1, p120ctn). *B*, RSK proximity partners identified and their association with specific cellular components. *C*, Gene ontology (GO) enrichments for cellular components and molecular functions. *D*, Venn diagram showing the overlap in identified proteins from BioID experiments and a previous RSK phosphoproteomic study (18).

specific antibody directed against this phosphorylation site. As expected, we found that potent agonists of the RAS/MAPK pathway, including PMA and EGF, robustly stimulated p120ctn phosphorylation at Ser320 in HEK293 cells (Fig. 4*A*). Conversely, activation of Akt, a basophilic kinase of the AGC family that shares common substrates with RSK (51), by serum or insulin, did not promote Ser320 phosphorylation (Fig. 4*A*). We also treated cells with increasing concentrations of insulin, but despite high Akt phosphorylation levels, we did not detect Ser320 phosphorylation (Fig. 4*B*), confirming that Akt does not regulate this phosphorylation site. Prolonged stimulation using PMA or EGF in HEK293 cells leads to a strong phosphorylation at Ser320 (Fig. 4*C*), confirming the

involvement of the RAS/MAPK pathway in this phosphorylation event. This was further confirmed using pharmacologic inhibitors in HEK293 cells. We found that MEK1/2 inhibition using PD184352 decreased Ser320 phosphorylation induced by PMA or EGF stimulation (Fig. 4*D*), whereas mTOR inhibitors (Ku-0063794, rapamycin) or a dual PI3K/mTOR inhibitor (PI-103) did not affect p120ctn phosphorylation. To confirm the involvement of RSK in Ser320 phosphorylation in cells, we used small interfering RNA (siRNA)-mediated RNA interference (RNAi) to specifically reduce RSK1 and RSK2 expression, the predominant RSK isoforms expressed in HEK293 cells. We found that knockdown of RSK1 and RSK2 significantly reduced p120ctn phosphorylation in response to PMA
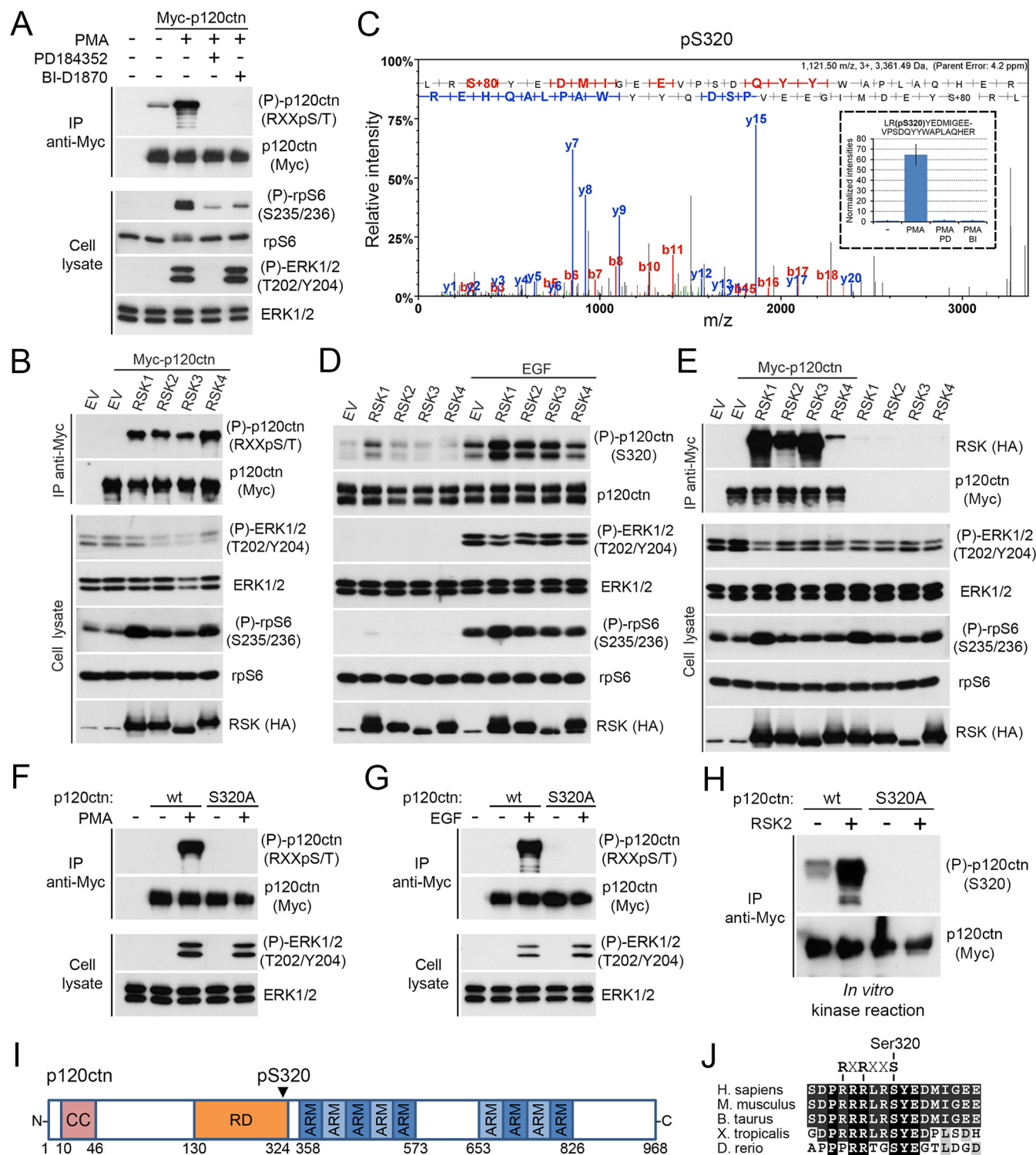
FIG. 3. **RSK phosphorylates p120ctn at Ser320.** *A*, HEK293 cells were transfected with an empty vector (EV) or Myc-tagged p120ctn, serum-starved overnight and pretreated with PD184352 (10 μM) or LJH685 (10 μM) for 30 min before PMA (100 ng/ml) stimulation. Immunoprecipitated (IP) Myc-p120ctn was then assayed for phosphorylation with a phosphomotif antibody that recognizes the RXXpS/T consensus. Protein lysates were resolved by SDS-PAGE and analyzed by immunoblotting with the indicated antibodies. *B*, As in (A), except that HA-tagged RSK1–4 were transfected along with Myc-p120ctn. Immunoprecipitated (IP) Myc-p120ctn was then assayed for phospho-rylation with a phosphomotif antibody that recognizes the RXXpS/T consensus. *C*, Phosphorylation of human p120ctn at Ser320 was confirmed via high-resolution MS/MS sequencing using immunoprecipitated p120ctn under the same conditions as in (A). After SDS-PAGE separation, bands corresponding to p120ctn were excised and proteins were digested in-gel with trypsin for relative quantification. (Inset) Relative
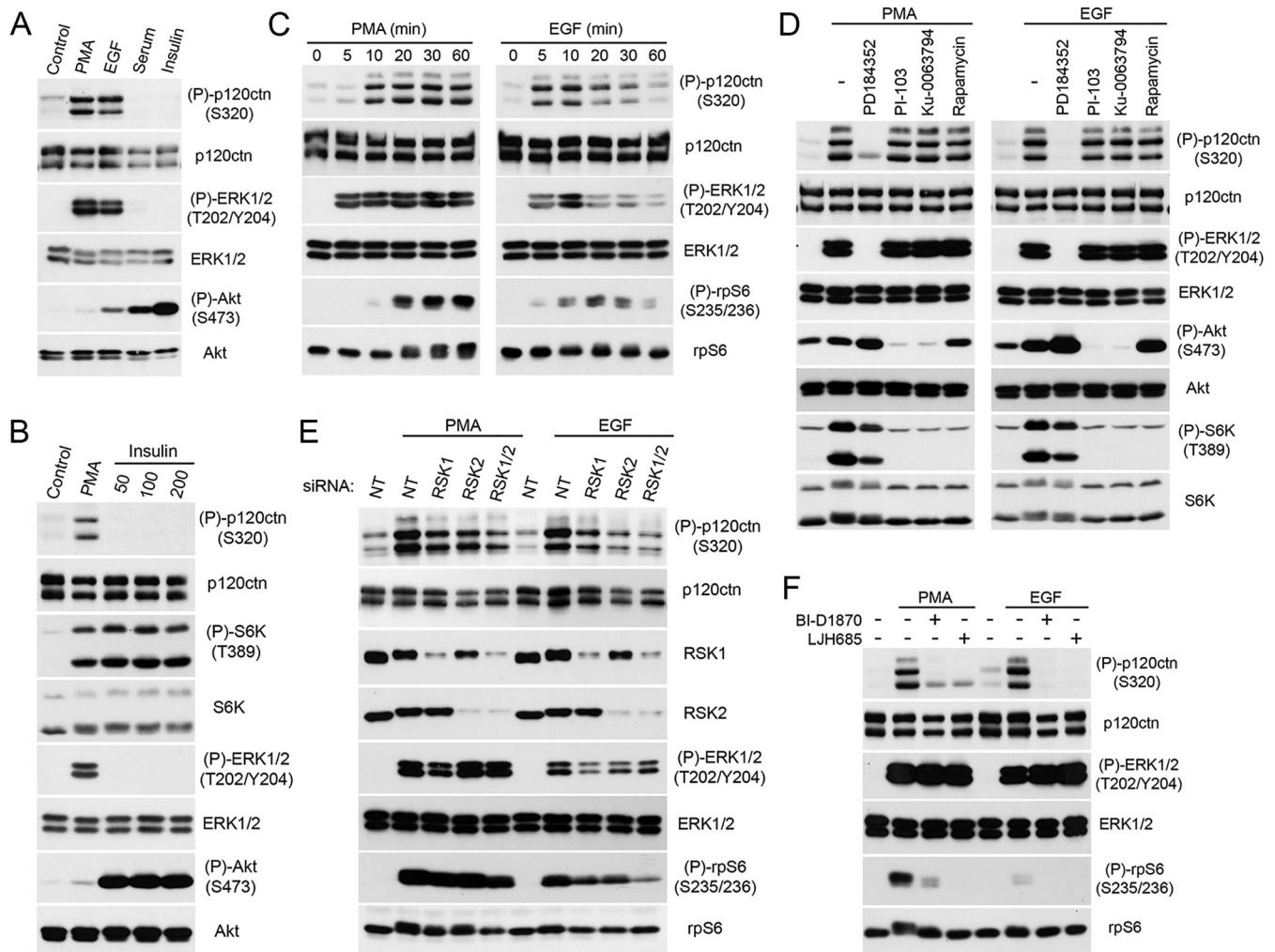
FIG. 4. **The Ras/MAPK pathway mediates Ser320 phosphorylation in a RSK-dependent manner.** *A*, HEK293 cells were serum-starved overnight before stimulation for 10–30 min with agonists of the Ras/MAPK (PMA, 100 ng/ml; EGF, 25 ng/ml) and PI3K/Akt (Insulin, 100 nM; FBS, 10%) pathways. Protein lysates were resolved by SDS-PAGE and analyzed by immunoblotting with the indicated antibodies. *B*, HEK293 cells were serum-starved overnight before PMA (100 ng/ml) or insulin stimulation at increasing concentrations ranging from 50 to 200 nM. Protein lysates were analyzed as in (*A*). *C*, HEK293 cells were serum-starved overnight before a time course of PMA (100 ng/ml) or EGF (25 ng/ml) stimulation. Extracts were prepared at the indicated times and analyzed as in (*A*). *D*, HEK293 cells were serum-starved overnight and pretreated with PD184352 (10 μM), PI-103 (1 μM), Ku-0063794 (10 μM) or rapamycin (25 nM) for 30 min before PMA (100 ng/ml) or EGF (25 ng/ml) stimulation. Protein lysates were analyzed as in (*A*). *E*, HEK293 cells were transfected with siRNAs targeted against a scrambled sequence (NT), RSK1, RSK2 or both, serum-starved and stimulated either with PMA (100 ng/ml) or EGF (25 ng/ml). Protein lysates were analyzed as in (*A*). *F*, HEK293 cells were serum-starved and pretreated with BI-D1870 (10 μM) or LJH685 (10 μM) for 30 min before PMA (100 ng/ml) or EGF (25 ng/ml) stimulation. Protein lysates were analyzed as in (*A*).

abundance of phosphorylated Ser320 across the four conditions normalized with respect to overall p120ctn abundance. *D*, HEK293 cells were transfected with HA-tagged RSK1–4, serum-starved overnight, and treated with EGF (25 ng/ml) for 10 min. Cell lysates were assessed for endogenous p120ctn phosphorylation using a phosphospecific antibody targeted against Ser320. *E*, HEK293 cells were co-transfected with Myc-p120ctn and HA-tagged RSK1–4. The presence of HA-tagged RSK1–4 was then assessed within Myc-p120ctn immunoprecipitates. Protein lysates were resolved by SDS-PAGE and analyzed by immunoblotting with the indicated antibodies. *F, G*, HEK293 cells were transfected with WT p120ctn or potential RSK phosphorylation site mutant (S320A), serum starved overnight, and stimulated with PMA (100 ng/ml) or EGF (25 ng/ml). Immunoprecipitated (IP) Myc-p120ctn and protein lysates were analyzed as in (*A*). H, Recombinant-active RSK2 was incubated with immunoprecipitated p120ctn WT or the non-phosphorylatable mutant S320A in a kinase reaction. Immunoprecipitated proteins were resolved by SDS-PAGE and analyzed by immunoblotting with the indicated antibodies. *I*, Schematic representation of p120ctn. CC, Coiled Coil; RD, Regulatory Domain; ARM, Armadillo-Repeats. *J*, Sequence surrounding Ser320 in p120ctn from various species were aligned to show the evolutionary conservation of the Ser320 residue within a RSK consensus motif (RXRXXS, where X is any amino acid).

or EGF stimulation (Fig. 4*E*). Knockdown of both RSK1 and RSK2 further reduced Ser320 phosphorylation compared with knockdown of RSK1 or RSK2 alone, suggesting that both isoforms may be responsible for p120ctn phosphorylation. As expected from the RNAi data, we confirmed that RSK is required for the phosphorylation of endogenous p120ctn in HEK293 cells, as two different RSK inhibitors (BI-D1870, LJH685) were found to reduce Ser320 phosphorylation after PMA or EGF stimulation (Fig. 4*F*). Taken together, these results confirm that RSK is required for p120ctn phosphorylation at Ser320 in response to agonists of the RAS/MAPK pathway.

p120ctn Maintains Cell-Cell Adhesion in BRAF-mutated Melanoma—Melanomas are characterized by the hyperactivation of the RAS/MAPK pathway (7, 52), and RSK activity was shown to be elevated in cells derived from this cancer subtype (19, 20). To determine if the RAS/MAPK pathway regulates p120ctn phosphorylation in melanoma cells, we tested several pathway inhibitors in BRAF-mutated cell lines (Colo829 and A375). As observed in HEK293 cells, we found that p120ctn phosphorylation was affected by MEK1/2 inhibition using PD184352, but not by mTOR inhibitors (Ku-0063794, rapamycin) or a dual PI3K/mTOR inhibitor (PI-103) (Fig. 5*A*). These results indicate that p120ctn phosphorylation is mainly regulated by the RAS/MAPK pathway in melanoma cells. We also found that treatment of A375 and Colo829 cells with RSK inhibitors (BI-D1870, LJH685, SL0101) abrogated p120ctn phosphorylation at Ser320 (Fig. 5*B*), indicating that RSK is the main kinase acting downstream of the RAS/MAPK pathway in BRAF-mutant melanoma cells. To confirm these results, we used a knockdown approach with lentiviral shRNAs targeted against two different sequences in both *RSK1* and *RSK2* mRNAs. Compared with a control shRNA (shNT) or shRNAs against RSK1 (shRSK1.1, shRSK1.2), we found that depletion of RSK2 (shRSK2.1, shRSK2.2) resulted in a significant decrease of Ser320 phosphorylation in serum-growing Colo829 (Fig. 5*C*), demonstrating that RSK2 is the predominant isoform regulating p120ctn phosphorylation in these cells. Finally, we investigated whether p120ctn is phosphorylated in human tissues and found by immunohistochemistry that Ser320 phosphorylation was increased in melanoma compared with adjacent normal skin (Fig. 5*D*), suggesting that this phosphorylation event has important functions in melanoma development.

Although p120ctn has been studied in many types of cancer (35), its role in melanoma remains elusive. To determine its importance in BRAF-mutated melanoma cells, we used a knockdown approach with lentiviral shRNAs. As expected (53), we found that depletion of p120ctn using two different shRNAs (p120ctn1, p120ctn2) reduced N-cadherin protein levels (Fig. 5*E*). We also assessed the subcellular localization of endogenous N-cadherin, and found that p120ctn knockdown decreased its plasma membrane localization while simultaneously increasing its cytoplasmic levels (Fig. 5*F*). These results indicate that p120ctn promotes the stability of N-cadherin at the plasma membrane of melanoma cells, as previously described in several other cell types (29). To determine if p120ctn regulates intercellular adhesion strength in melanoma cells, A375 cells subjected to p120ctn knockdown were lifted using dispase and tissue fragmentation calculated following mechanical stress (number of single cells/total cell number) (54, 55). We found that depletion of p120ctn using two different shRNAs increased cell fragmentation (Fig. 5*G*), indicating that p120ctn is required for melanoma cell-cell adhesion.

RSK Negatively Regulates Cell-Cell Junctions in Melanoma—Although the RAS/MAPK pathway regulates diverse biological processes, few studies have addressed its role in the regulation of cell-cell adherence. RSK was shown to promote the transition from multicellular epithelium to single cell phenotype, but these effects were found to be transcription-dependent (56, 57). To determine if RSK regulates melanoma cell-cell adhesion, we performed a fragmentation assay on cells subjected to RSK1/2 knockdown or treated with pharmacological inhibitors. Consistent with a role for RSK in cell-cell adhesion, we found that knockdown of both RSK1 and RSK2 (shRSK1/2) significantly reduced A375 cell fragmentation (Fig. 6*A*). We also evaluated A375 cells pretreated with either vehicle (DMSO), MEK1/2 (PD184352) or RSK (LJH685) inhibitors (Fig. 6*B* and 6*C*), and found that cell fragmentation was reduced by RSK inhibition. Taken together, these results indicate that the RAS/MAPK pathway and RSK negatively regulate intercellular junctions.

Our results indicate that p120ctn is required for melanoma cell-cell adhesion, and that RSK constitutively phosphorylates Ser320 in these cells. As we found that RSK also regulates melanoma cell-cell adherence, we assessed the role of p120ctn phosphorylation in this cellular process. First, we evaluated the subcellular localization of endogenous p120ctn and N-cadherin in A375 cells treated with either vehicle (DMSO), MEK1/2 (PD184352) or RSK (LJH685) inhibitors (Fig. 6*D*). We found that both p120ctn and N-cadherin did not change localization in response to RSK inhibition, suggesting that Ser320 phosphorylation does not regulate p120ctn localization. To determine if RSK regulates the interaction between p120ctn and N-cadherin, melanoma cells were treated with MEK1/2 (PD184352) and RSK (LJH685) inhibitors prior to p120ctn immunoprecipitation. Consistent with the subcellular localization results, we found that RSK inhibition did not affect N-cadherin binding to p120ctn (Fig. 6*E*). To specifically evaluate the role of Ser320 phosphorylation, we generated stable A375 cell lines expressing either GFP, wild-type p120ctn (WT), or the non-phosphorylatable (S320A) or potential phosphomimetic (S320D) mutants. The stable cell lines were depleted for endogenous p120ctn using an shRNA targeting the 3′UTR of the endogenous p120ctn mRNA and assessed for cell-cell adhesion using the fragmentation assay. Although p120ctn depletion increased the fragmentation of GFP-ex-
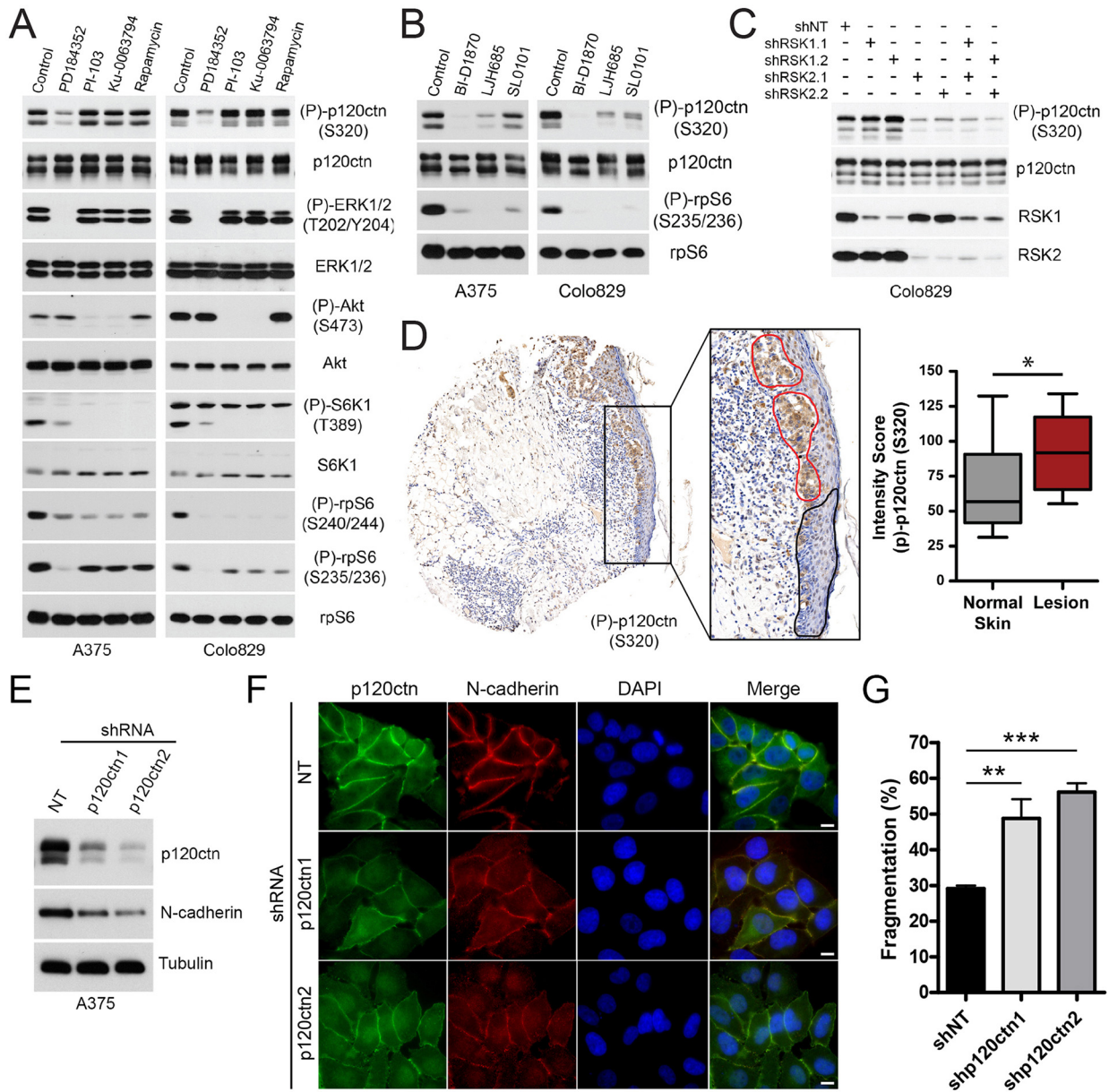
FIG. 5. **p120ctn is phosphorylated at Ser320 and maintains cell-cell adhesion in BRAF-mutated melanoma cells.** *A*, A375 and Colo829 cells were serum-starved overnight and pretreated with PD184352 (10 μM), PI-103 (1 μM), Ku-0063794 (10 μM) or rapamycin (25 nM) for 30 min. Endogenous p120ctn phosphorylation was assessed by immunoblotting. *B*, Same as (*A*), except that A375 and Colo829 cells were treated with LJH685 (10 μM), BI-D1870 (10 μM) or SL0101 (50 μM) for 30 min. *C*, RNAi was performed in Colo829 cells with shRNAs against RSK1 (shRSK1.1 or shRSK1.2) or RSK2 (shRSK2.1 or shRSK2.2) or both, to generate stable knockdowns. shRNA efficiency and p120ctn phosphorylation was then evaluated through immunoblotting with the indicated antibodies. *D*, IHC analysis of p120ctn phosphorylated on S320 in human melanoma tissue microarrays. A representative image of normal skin adjacent to melanoma tissues shows increased labeling with the phospho-Ser320 antibody. For each case analyzed, the labeling was quantified and compared between normal skin (black) and melanoma lesions (red). Values represent the quantification of phospho-Ser320 from nine individual patients. *E*, A375 cells were knocked down for p120ctn using two different shRNA constructs (p120ctn1 or 2). shRNA efficiency was assessed by immunoblotting with the anti-p120ctn antibody. *F*, Immunofluorescence images of growing A375 cells stably expressing a control shRNA (shNT) or shRNAs against p120ctn (shp120ctn1 or 2). Cells were stained with anti-p120ctn to monitor p120ctn expression, with anti-N-cadherin to monitor N-cadherin expression and DAPI to visualize nuclei. Scale bars, 10 μm. *G*, Dispase treatment caused separation of the monolayer in all cells treated. Mechanical stress following dispase treatment led to the breakdown of A375 cells stably expressing a control shRNA (shNT) or shRNAs against p120ctn (shp120ctn1 or 2). Bar graph showing the average number of single cells recorded under the three conditions tested. $n = 3$ for all conditions. Fragmentation was calculated based on the ratio of single cell over the total cell number per plate. Statistically significant changes are indicated by asterisks (*, $p < 0.05$; **, $p < 0.01$; ***, $p < 0.001$ by unpaired Student t test).
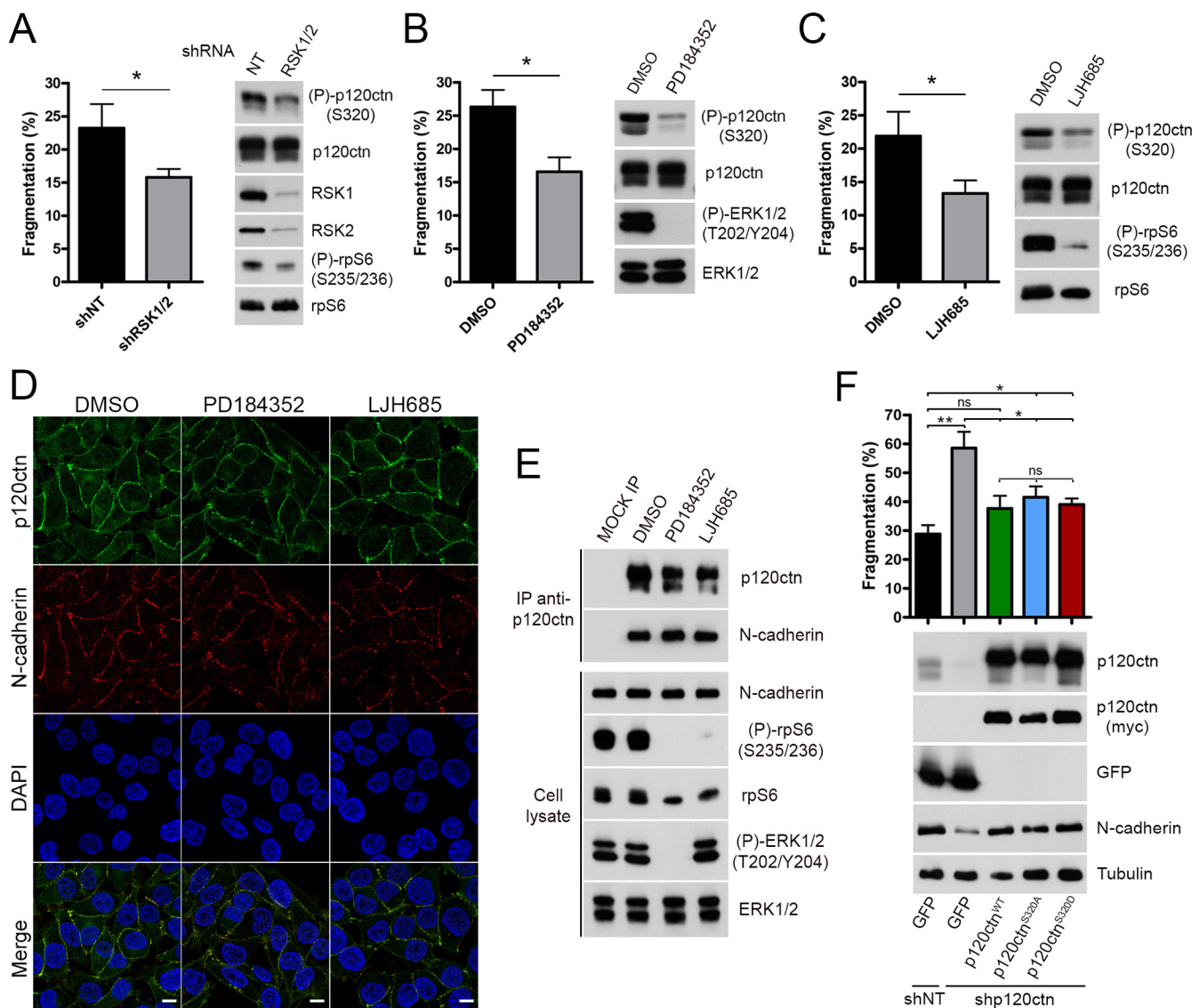
FIG. 6. **RSK regulates intercellular adhesion strength.** *A*, Dispase treatment caused separation of the monolayer in all cells treated. Mechanical stress following dispase led to the breakdown of A375 cells stably expressing a control shRNA (shNT) or shRNA against RSK1/2 (shRSK1/2). Bar graph showing the average number of single cells recorded under the three conditions tested. *n* = 3 for all conditions. Protein lysates from each condition were analyzed by immunoblotting with the indicated antibodies. *B*, *C*, As in (*A*), except that A375 cells were pretreated during 24 h with PD184352 (10 µM) or LJH685 (10 µM) before dispase treatment. *D*, A375 were imaged using immunofluorescence microscopy after a treatment with PD184352 (10 µM) or LJH685 (10 µM) for 24 h. Cells were stained with anti-p120ctn to monitor p120ctn expression, with anti-N-cadherin to monitor N-cadherin expression and DAPI to visualize nuclei. Scale bars, 10 µm. *E*, A375 cells were treated with PD184352 (10 µM) or LJH685 (10 µM) for 24 h. p120ctn was immunoprecipitated with anti-p120ctn antibody, and immunoblotting was performed on immunoprecipitates and cell lysates using indicated antibodies. *F*, As in (*A*), except that A375 cells were stably expressing a control shRNA (shNT) and GFP protein, or an shRNA against the 3'UTR of endogenous p120ctn and GFP protein or exogenous form of p120ctn (p120ctn^{WT}, p120ctn^{S320A} or p120ctn^{S320D}) before dispase treatment. Bottom part shows protein lysates from each condition analyzed by immunoblotting with the indicated antibodies. Depletion or expression of endogenous/exogenous p120ctn in each condition was assessed using the p120ctn antibody. Statistically significant changes are indicated by asterisks (*, *p* < 0.05; **, *p* < 0.01; ***, *p* < 0.001 by unpaired Student *t* test).

pressing cells, we found that all three p120ctn alleles rescued cell-cell adhesion to the same extent (Fig. 6*F*). These results suggest that Ser320 phosphorylation does not regulate p120ctn-mediated cell-cell adhesion, which is consistent with the ability of each p120ctn allele to rescue N-cadherin expres-

sion in response to p120ctn knockdown (Fig. 6*F*). Together, these results indicate that, although p120ctn and RSK regulate melanoma cell-cell adhesion, the role of Ser320 phosphorylation remains elusive and additional approaches are required to elucidate its function.

Phosphorylation of p120ctn at Ser320 Regulates Its Cellular Proximity Partners—To investigate the potential role of p120ctn phosphorylation at Ser320, we generated stable HEK293 Flp-In T-Rex cell lines expressing wild-type p120ctn (WT), or the S320A and S320D mutants fused in-frame with the promiscuous biotin ligase BirA (R118G). These cell lines were found to express similar levels of fusion proteins and exhibited similar protein biotinylation patterns (Fig. 7A). Using these cells, we performed a BioID analysis and found significant proximity partners (SAINT score > 0.5 and FDR < 0.1) for wild-type p120ctn (WT) (98), as well as the S320A (107) and S320D (76) mutants (supplemental Tables S3B, S5). Although ~25% of identified proteins were common to the three different baits, we identified several specific proximity partners (Fig. 7B). Common proximity partners include several known p120ctn interactors, such CDH2 (N-cadherin), CTNNA1 (α-catenin), CTNNB1 (β-catenin) and PLEKHA7 (35, 58). In addition to proteins involved in adherens junctions and cytoskeletal organization, our results suggest that p120ctn associate with several proteins involved in RNA metabolism (Fig. 7C). Among these, we found LSM14A, EIF4ENIF1 (4E-T) and AGO2, which were mainly identified as preys of the p120ctn S320D mutant. Using confocal microscopy, we confirmed the co-localization of p120ctn and 4E-T near intercellular junctions, as confirmed by analyzing Z-stack projections and by monitoring relative fluorescence intensity across a field (Fig. 7D and 7E). We further confirmed these results by showing the correlation ($r = 0.503$) between p120ctn and 4E-T pixels (Fig. 7F). Together, these results suggest that Ser320 phosphorylation may affect several aspects of p120ctn function, including new functions in RNA metabolism that have not yet been explored.

DISCUSSION

In this study, we describe the first global *in vivo* proximity labeling study of the RSK protein kinases (Fig. 1 and 2). Using BioID, we identified several potential cellular partners, including p120ctn, a member of the Armadillo-repeat protein family. We characterized p120ctn as a new RSK substrate (Fig. 3, 4 and 5), and we found that phosphorylation at Ser320 potentially modifies its proximity cellular partners (Fig. 7). Notably, we reveal that p120ctn colocalizes with 4E-T at sites of cell-cell adhesion, suggesting that p120ctn regulates RNA silencing within this cellular compartment (Fig. 7). Importantly, we also demonstrate the key role played by p120ctn in melanoma cell-cell junctions (Fig. 5), and we show that RSK negatively regulates AJ integrity (Fig. 6).

The BioID approach identifies proximity partners that are within a 10–20-nm radius from the bait fused to BirA (47), and thereby provides information about the localization of bait proteins. Most of the proteins identified using RSK as bait were found to localize at the plasma membrane and have roles related to this cellular compartment (Fig. 2). These results are interesting because the majority of RSK substrates

identified so far were not shown to localize to the plasma membrane (9). However, our results support several studies reporting a potential role for RSK at the plasma membrane, including the phosphorylation of Filamin A (59, 60), which is involved in the stabilization of actin cortex. Also, most membrane-associated proteins were identified using RSK3 as bait (Fig. 2), suggesting a specific role for RSK3 at this cellular compartment. Interestingly, we found that all four RSK isoforms associate with p120ctn by co-immunoprecipitation. At first glance, these results appear contradictory to BioID results showing a specificity toward RSK3 but may suggest that RSK3 spends more time in the vicinity of p120ctn than any other RSK isoforms. Notwithstanding the possibility that these apparent discrepancies could be false negative results from BioID experiments, our additional data clearly indicate that all four RSK isoforms appear to phosphorylate p120ctn in cells.

By controlling the stability of cadherins at the plasma membrane, p120ctn maintains cell-cell adhesion (27–29). Negative regulation and/or mis-localization of p120ctn have been reported in many cancers, leading most of the time to the emergence of the epithelial-mesenchymal transition (EMT) process (35). Our results suggest the importance of p120ctn in maintaining intercellular junctions in melanoma cells (Fig. 5). We identified Ser320 as a novel p120ctn phosphorylation site and demonstrated its regulation by the RAS/MAPK pathway and more specifically, RSK (Fig. 3 and 4). This phosphorylation event was found to modify the proximity partners of p120ctn (Fig. 7). Indeed, our data suggest that p120ctn phosphorylation at Ser320 promotes its relocalization to P-bodies (Fig. 7). Finally, we show that Ser320 phosphorylation is increased in human melanomas (Fig. 5D), suggesting that this phosphorylation may be used as a biological marker for melanoma development. This corroborates with several studies showing that phosphorylated p120ctn expression has a predictive value for cancer progression (34).

Using the cell fragmentation approach, we found that inhibition of RSK activity promotes the maintenance of intercellular junctions (Fig. 6A–6C). These results suggest that tumor cells with deregulated RSK activity, such as melanoma, may have weaker intercellular junctions, but these effects do not seem to require p120ctn phosphorylation at Ser320. RSK may promote cell fragmentation by regulating other substrates at the plasma membrane, as several proximity interactors identified may play some roles in AJ maintenance. Additional studies will be required to decipher the underlying molecular mechanisms mediating the effect of RSK on the integrity of intercellular junctions.

Using BioID, we were able to identify two known functional clusters of p120ctn involved in cell-cell adhesion and cytoskeletal organization (Fig. 7C). We also found a new protein cluster involved in translational regulation and RNA interference, which may be affected by p120ctn phosphorylation status. Recent studies have shown that p120ctn interacts with PLEKHA7, which recruits AGO2, GW182, PABPC1 and sev-
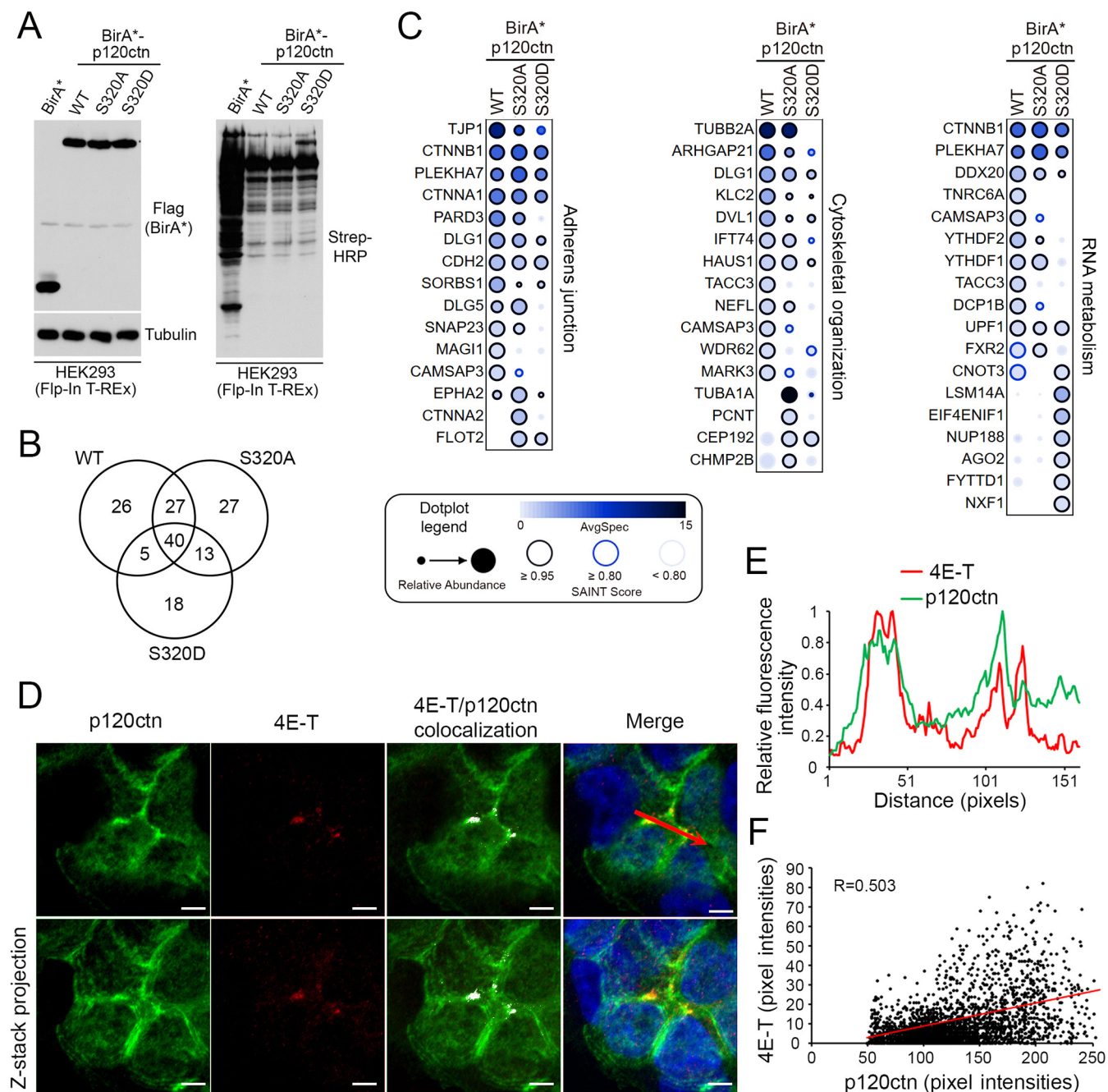
FIG. 7. **p120ctn proximity partners are regulated by Ser320 phosphorylation.** *A*, HEK293 Flp-In T-REx stable cell lines were treated with tetracycline in the presence of biotin for 24 h to induce bait expression and proximity biotinylation. Bait expression and biotinylation patterns were monitored using a Flag antibody and Streptavidin-HRP, respectively. *B*, Venn diagram showing the overlap of proximity interactors identified by BioID with the three different baits. Only the preys with a SAINT Score > 0.5 were considered. *C*, Dotplot of selected interaction partners identified by BioID. The node color represents the average spectral count sum ($n = 3$), the node edge color corresponds to the SAINT Score and the node size displays the relative abundance of a given prey across the three conditions compared. *D*, A375 cells were stained for endogenous p120ctn (green) and 4E-T (red), and pictures were taken with a confocal microscope. White dots represent p120ctn and 4E-T colocalization. *E*, Graph representing the relative fluorescence intensity of 4E-T and p120ctn along the area shown by the red arrow in (*D*). *F*, Scatter plot representing the correlation between in p120ctn and 4E-T staining. The red line represents the Pearson correlation trendline. Scale bars, 10 μm.

eral accessory proteins of the RNA-induced silencing complex (RISC) (61). Our results suggest that the RNA transporter 4E-T, which was shown to enhance RNA silencing (62), may also be part of this complex (63). We found that p120ctn and 4E-T colocalize near sites of cell-cell adhesion, suggesting that 4E-T regulates RNA silencing within adherens junctions. More

experimentation will be required to address the role of p120ctn phosphorylation at Ser320 in the regulation of RNA silencing.

In conclusion, our study reveals the robust and comprehensive power of our proteomic approach to identify potential RSK substrates and cellular partners. Our results implicating RSK in the regulation of p120ctn and cell-cell adhesion support the possibility that RSK may be a valuable therapeutic target against cancer. Our proteomic findings also suggest that the RSK isoforms play various biological functions downstream of the RAS/MAPK pathway, and that many more RSK cellular partners remain to be characterized.

DATA AVAILABILITY

All raw mass spectrometry data have been deposited at MassIVE (massive.ucsd.edu; accession number MSV000083414 and PXD012619). It can be downloaded from ftp://massive.ucsd.edu/MSV000083414/.

REFERENCES

1. Cargnello, M., and Roux, P. P. (2011) Activation and function of the MAPKs and their substrates, the MAPK-activated protein kinases. *Microbiol. Mol. Biol. Rev.* **75,** 50–83
2. Meloche, S., and Pouyssegur, J. (2007) The ERK1/2 mitogen-activated protein kinase pathway as a master regulator of the G1- to S-phase transition. *Oncogene* **26,** 3227–3239
3. Nussinov, R., Tsai, C. J., Chakrabarti, M., and Jang, H. (2016) A New View of Ras Isoforms in Cancers. *Cancer Res.* **76,** 18–23
4. Takashima, A., and Faller, D. V. (2013) Targeting the RAS oncogene. *Expert Opinion Therapeutic Targets* **17,** 507–531
5. Lavoie, H., and Therrien, M. (2015) Regulation of RAF protein kinases in ERK signalling. *Nature Reviews* **16,** 281–298
6. Roux, P., and Blenis, J. (2004) ERK and p38 MAPK-activated protein kinases: a family of protein kinases with diverse biological functions. *Microbiol. Mol. Biol. Rev.* **68,** 320–344
7. Michaloglou, C., Vredeveld, L. C., Mooi, W. J., and Peeper, D. S. (2008) BRAF(E600) in benign and malignant human tumours. *Oncogene* **27,** 877–895
8. Romeo, Y., and Roux, P. P. (2011) Paving the way for targeting RSK in cancer. *Expert Opinion Therapeutic Targets* **15,** 5–9
9. Romeo, Y., Zhang, X., and Roux, P. P. (2012) Regulation and function of the RSK family of protein kinases. *Biochemical J.* **441,** 553–569
10. Carriere, A., Ray, H., Blenis, J., and Roux, P. P. (2008) The RSK factors of activating the Ras/MAPK signaling cascade. *Front Biosci.* **13,** 4258–4275
11. Anjum, R., Roux, P., Ballif, B., Gygi, S., and Blenis, J. (2005) The tumor suppressor DAP kinase is a target of RSK-mediated survival signaling. *Curr. Biol.* **15,** 1762–1767
12. Roux, P., Ballif, B., Anjum, R., Gygi, S., and Blenis, J. (2004) Tumor-promoting phorbol esters and activated Ras inactivate the tuberous sclerosis tumor suppressor complex via p90 ribosomal S6 kinase. *Proc. Natl. Acad. Sci. U.S.A.* **101,** 13489–13494
13. Roux, P. P., Shahbazian, D., Vu, H., Holz, M. K., Cohen, M. S., Taunton, J., Sonenberg, N., and Blenis, J. (2007) RAS/ERK signaling promotes site-specific ribosomal protein S6 phosphorylation via RSK and stimulates cap-dependent translation. *Biol. Chem.* **282,** 14056–14064
14. Sulzmaier, F. J., Young-Robbins, S., Jiang, P., Geerts, D., Prechtl, A. M., Matter, M. L., Kesari, S., and Ramos, J. W. (2016) RSK2 activity mediates glioblastoma invasiveness and is a potential target for new therapeutics. *Oncotarget* **7,** 9869–79884
15. Cuesta, R., and Holz, M. K. (2016) RSK-mediated down-regulation of PDCD4 is required for proliferation, survival, and migration in a model of triple-negative breast cancer. *Oncotarget* **7,** 27567–27583
16. Clark, D. E., Errington, T. M., Smith, J. A., Frierson, H. F., Jr, Weber, M. J., and Lannigan, D. A. (2005) The serine/threonine protein kinase, p90 ribosomal S6 kinase, is an important regulator of prostate cancer cell proliferation. *Cancer Res.* **65,** 3108–3116
17. Kang, S., Elf, S., Lythgoe, K., Hitosugi, T., Taunton, J., Zhou, W., Xiong, L., Wang, D., Muller, S., Fan, S., Sun, S. Y., Marcus, A. I., Gu, T. L., Polakiewicz, R. D., Chen, Z. G., Khuri, F. R., Shin, D. M., and Chen, J. (2010) p90 ribosomal S6 kinase 2 promotes invasion and metastasis of human head and neck squamous cell carcinoma cells. *J. Clin. Investigation* **120,** 1165–1177
18. Galan, J. A., Geraghty, K. M., Lavoie, G., Kanshin, E., Tcherkezian, J., Calabrese, V., Jeschke, G. R., Turk, B. E., Ballif, B. A., Blenis, J., Thibault, P., and Roux, P. P. (2014) Phosphoproteomic analysis identifies the tumor suppressor PDCD4 as a RSK substrate negatively regulated by 14–3-3. *Proc. Natl. Acad. Sci. U.S.A.* **111,** E2918–E2927
19. Houles, T., Gravel, S.-P., Lavoie, G., Shin, S., Savall, M., Meant, A., Grondin, B., Gaboury, L., Yoon, S.-O., St-Pierre, J., and Roux, P. P. (2018) RSK regulates PFK-2 activity to promote metabolic rewiring in melanoma. *Cancer Res.* **78,** 2191–2204
20. Romeo, Y., Moreau, J., Zindy, P.-J., Saba-El-Leil, M., Lavoie, G., Dandachi, F., Baptissart, M., Borden, K. L. B., Meloche, S., and Roux, P. P. (2013) RSK regulates activated BRAF signalling to mTORC1 and promotes melanoma growth. *Oncogene* **32,** 2917–2926
21. Bignone, P. A., Lee, K. Y., Liu, Y., Emilion, G., Finch, J., Soosay, A. E., Charnock, F. M., Beck, S., Dunham, I., Mungall, A. J., and Ganesan, T. S. (2007) RPS6KA2, a putative tumour suppressor gene at 6q27 in sporadic epithelial ovarian cancer. *Oncogene* **26,** 683–700
22. Cai, J., Ma, H., Huang, F., Zhu, D., Zhao, L., Yang, Y., Bi, J., and Zhang, T. (2014) Low expression of RSK4 predicts poor prognosis in patients with colorectal cancer. *Int. J. Clin. Exp. Pathol.* **7,** 4959–4970
23. Houles, T., and Roux, P. P. (2017) Defining the role of the RSK isoforms in cancer. *Sem. Cancer Biol.* **48,** 3–61.
24. Schneider, M. R., and Kolligs, F. T. (2015) E-cadherin's role in development, tissue homeostasis and disease: Insights from mouse models: Tissue-specific inactivation of the adhesion protein E-cadherin in mice reveals its functions in health and disease. *Bioessays* **37,** 294–304
25. Halbleib, J. M., and Nelson, W. J. (2006) Cadherins in development: cell adhesion, sorting, and tissue morphogenesis. *Genes Development* **20,** 3199–3214
26. Gumbiner, B. M. (2005) Regulation of cadherin-mediated adhesion in morphogenesis. *Nature Rev.* **6,** 622–634
27. Rimm, D. L., Koslov, E. R., Kebriaei, P., Cianci, C. D., and Morrow, J. S. (1995) Alpha 1(E)-catenin is an actin-binding and -bundling protein mediating the attachment of F-actin to the membrane adhesion complex. *Proc. Natl. Acad. Sci. U.S.A.* **92,** 8813–8817
28. Valenta, T., Hausmann, G., and Basler, K. (2012) The many faces and functions of beta-catenin. *EMBO J.* **31,** 2714–2736

29. Davis, M. A., Ireton, R. C., and Reynolds, A. B. (2003) A core function for p120-catenin in cadherin turnover. *J. Cell Biol.* **163,** 525–534

30. Carnahan, R. H., Rokas, A., Gaucher, E. A., and Reynolds, A. B. (2010) The molecular evolution of the p120-catenin subfamily and its functional associations. *PloS One* **5,** e15747

31. Alema, S., and Salvatore, A. M. (2007) p120 catenin and phosphorylation: Mechanisms and traits of an unresolved issue. *Biochim. Biophys. Acta* **1773,** 47–58

32. Fukumoto, Y., Shintani, Y., Reynolds, A. B., Johnson, K. R., and Wheelock, M. J. (2008) The regulatory or phosphorylation domain of p120 catenin controls E-cadherin dynamics at the plasma membrane. *Exp. Cell Res.* **314,** 52–67

33. Peglion, F., Llense, F., and Etienne-Manneville, S. (2014) Adherens junction treadmilling during collective migration. *Nat. Cell Biol.* **16,** 639–651

34. Kourtidis, A., Yanagisawa, M., Huveldt, D., Copland, J. A., and Anastasiadis, P. Z. (2015) Pro-tumorigenic phosphorylation of p120 catenin in renal and breast cancer. *PloS one* **10,** e0129964

35. van Hengel, J., and van Roy, F. (2007) Diverse functions of p120ctn in tumors. *Biochim. Biophys. Acta* **1773,** 78–88

36. Carriere, A., Cargnello, M., Julien, L. A., Gao, H., Bonneil, E., Thibault, P., and Roux, P. P. (2008) Oncogenic MAPK signaling stimulates mTORC1 activity by promoting RSK-mediated raptor phosphorylation. *Current Biol.* **18,** 1269–1277

37. Kean, M. J., Couzens, A. L., and Gingras, A. C. (2012) Mass spectrometry approaches to study mammalian kinase and phosphatase associated proteins. *Methods* **57,** 400–408

38. Kessner, D., Chambers, M., Burke, R., Agus, D., and Mallick, P. (2008) ProteoWizard: open source software for rapid proteomics tools development. *Bioinformatics* **24,** 2534–2536

39. Shteynberg, D., Deutsch, E. W., Lam, H., Eng, J. K., Sun, Z., Tasman, N., Mendoza, L., Moritz, R. L., Aebersold, R., and Nesvizhskii, A. I. (2011) iProphet: multi-level integrative analysis of shotgun proteomic data improves peptide and protein identification rates and error estimates. *Mol. Cell. Proteomics* **10,** M111.007690

40. Liu, G., Zhang, J., Larsen, B., Stark, C., Breitkreutz, A., Lin, Z. Y., Breitkreutz, B. J., Ding, Y., Colwill, K., Pasculescu, A., Pawson, T., Wrana, J. L., Nesvizhskii, A. I., Raught, B., Tyers, M., and Gingras, A. C. (2010) ProHits: integrated software for mass spectrometry-based interaction proteomics. *Nat. Biotechnol.* **28,** 1015–1017

41. Eng, J., McCormack, A., and Yates, J. R. (1994) An approach to correlate tandem mass spectral data of peptides with amino acid sequences in a protein database. *J. Am. Soc. Mass Spectrom.* **5,** 1579–1583

42. Keller, A., Nesvizhskii, A. I., Kolker, E., and Aebersold, R. (2002) Empirical statistical model to estimate the accuracy of peptide identifications made by MS/MS and database search. *Anal. Chem.* **74,** 5383–5392

43. Teo, G., Liu, G., Zhang, J., Nesvizhskii, A. I., Gingras, A. C., and Choi, H. (2014) SAINTexpress: improvements and additional features in Significance Analysis of INTeractome software. *J. Proteomics* **100,** 37–43

44. Mellacheruvu, D., Wright, Z., Couzens, A. L., Lambert, J. P., St-Denis, N. A., Li, T., Miteva, Y. V., Hauri, S., Sardiu, M. E., Low, T. Y., Halim, V. A., Bagshaw, R. D., Hubner, N. C., Al-Hakim, A., Bouchard, A., Faubert, D., Fermin, D., Dunham, W. H., Goudreault, M., Lin, Z. Y., Badillo, B. G., Pawson, T., Durocher, D., Coulombe, B., Aebersold, R., Superti-Furga, G., Colinge, J., Heck, A. J., Choi, H., Gstaiger, M., Mohammed, S., Cristea, I. M., Bennett, K. L., Washburn, M. P., Raught, B., Ewing, R. M., Gingras, A. C., and Nesvizhskii, A. I. (2013) The CRAPome: a contaminant repository for affinity purification-mass spectrometry data. *Nat. Methods* **10,** 730–736

45. Knight, J. D. R., Choi, H., Gupta, G. D., Pelletier, L., Raught, B., Nesvizhskii, A. I., and Gingras, A. C. (2017) ProHits-viz: a suite of web tools for visualizing interaction proteomics data. *Nat. Methods* **14,** 645–646

46. Shevchenko, A., Wilm, M., Vorm, O., and Mann, M. (1996) Mass spectrometric sequencing of proteins silver-stained polyacrylamide gels. *Anal. Chem.* **68,** 850–858

47. Roux, K. J., Kim, D. I., Burke, B., and May, D. G. (2018) BioID: A Screen for Protein-Protein Interactions. *Curr. Protoc. Protein Sci.* **91,** 19.23.1–19.23.15

48. Chatr-Aryamontri, A., Oughtred, R., Boucher, L., Rust, J., Chang, C., Kolas, N. K., O'Donnell, L., Oster, S., Theesfeld, C., Sellam, A., Stark, C., Breitkreutz, B. J., Dolinski, K., and Tyers, M. (2017) The BioGRID interaction database: 2017 update. *Nucleic Acids Res* **45,** D369–D379

49. Shi, G. X., Yang, W. S., Jin, L., Matter, M. L., and Ramos, J. W. (2018) RSK2 drives cell motility by serine phosphorylation of LARG and activation of Rho GTPases. *Proc. Natl. Acad. Sci. U.S.A.* **115,** E190–E199

50. Zhou, Y., Yamada, N., Tanaka, T., Hori, T., Yokoyama, S., Hayakawa, Y., Yano, S., Fukuoka, J., Koizumi, K., Saiki, I., and Sakurai, H. (2015) Crucial roles of RSK in cell motility by catalysing serine phosphorylation of EphA2. *Nat. Commun.* **6,** 7679

51. Moritz, A., Li, Y., Guo, A., Villen, J., Wang, Y., MacNeill, J., Kornhauser, J., Sprott, K., Zhou, J., Possemato, A., Ren, J. M., Hornbeck, P., Cantley, L. C., Gygi, S. P., Rush, J., and Comb, M. J. (2010) Akt-RSK-S6 kinase signaling networks activated by oncogenic receptor tyrosine kinases. *Sci. Signaling* **3,** ra64

52. Dhomen, N., and Marais, R. (2007) New insight into BRAF mutations in cancer. *Current Opinion Genetics Development* **17,** 31–39

53. Seidel, B., Braeg, S., Adler, G., Wedlich, D., and Menke, A. (2004) E- and N-cadherin differ with respect to their associated p120ctn isoforms and their ability to suppress invasive growth in pancreatic cancer cells. *Oncogene* **23,** 5532–5542

54. Sato, P. Y., Coombs, W., Lin, X., Nekrasova, O., Green, K. J., Isom, L. L., Taffet, S. M., and Delmar, M. (2011) Interactions between ankyrin-G, Plakophilin-2, and Connexin43 at the cardiac intercalated disc. *Circulation Res.* **109,** 193–201

55. Wei, Q., and Huang, H. (2014) Characterization of partially lifted cell sheets. *Tissue Eng. Part A* **20,** 1703–1714

56. Doehn, U., Hauge, C., Frank, S. R., Jensen, C. J., Duda, K., Nielsen, J. V., Cohen, M. S., Johansen, J. V., Winther, B. R., Lund, L. R., Winther, O., Taunton, J., Hansen, S. H., and Frodin, M. (2009) RSK is a principal effector of the RAS-ERK pathway for eliciting a coordinate promotile/invasive gene program and phenotype in epithelial cells. *Mol. Cell* **35,** 511–522

57. Caslavsky, J., Klimova, Z., and Vomastek, T. (2013) ERK and RSK regulate distinct steps of a cellular program that induces transition from multicellular epithelium to single cell phenotype. *Cellular signalling* **25,** 2743–2751

58. Peglion, F., and Etienne-Manneville, S. (2013) p120catenin alteration in cancer and its role in tumour invasion. *Philos. Trans. R. Soc. Lond. B Bio.l Sci.* **368,** 20130015

59. Gawecka, J. E., Young-Robbins, S. S., Sulzmaier, F. J., Caliva, M. J., Heikkila, M. M., Matter, M. L., and Ramos, J. W. (2012) RSK2 protein suppresses integrin activation and fibronectin matrix assembly and promotes cell migration. *J. Biol. Chem.* **287,** 43424–43437

60. Woo, M. S., Ohta, Y., Rabinovitz, I., Stossel, T. P., and Blenis, J. (2004) Ribosomal S6 Kinase (RSK) Regulates Phosphorylation of Filamin A on an Important Regulatory Site. *Mol. Cell. Biol.* **24,** 3025–3035

61. Kourtidis, A., Necela, B., Lin, W. H., Lu, R., Feathers, R. W., Asmann, Y. W., Thompson, E. A., and Anastasiadis, P. Z. (2017) Cadherin complexes recruit mRNAs and RISC to regulate epithelial cell signaling. *J. Cell Biol.* **216,** 3073–3085

62. Kamenska, A., Lu, W. T., Kubacka, D., Broomhead, H., Minshall, N., Bushell, M., and Standart, N. (2014) Human 4E-T represses translation of bound mRNAs and enhances microRNA-mediated silencing. *Nucleic Acids Res.* **42,** 3298–3313

63. Kourtidis, A., and Anastasiadis, P. Z. (2018) Close encounters of the RNAi kind: the silencing life of the adherens junctions. *Curr. Opin. Cell Biol.* **54,** 30–36